Measuring electron affinities with the photodetachment microscope

Christophe Valli, Christophe Blondel, and Christian Delsart
Laboratoire Aimé-Cotton, CNRS II, Bâtiment 505, F-91405 Orsay Cedex, France
(Received 8 December 1998)

Photodetachment microscopy, which was originally proposed as a new method for direct measurements of ionization or detachment energies, has been applied for a determination of the electron affinity of oxygen. The electron affinities of ^{16}O and ^{18}O could be measured separately from a natural sample. The experimental values (obtained as wave numbers, to be multiplied by hc to give energy units) are 11 784.682 (20) and 11 784.612 (29) cm^{-1}, respectively. The measured $^2P_{1/2}$-$^2P_{3/2}$ fine structure of $^{16}O^-$ is 177.085 (27) cm^{-1}. The observed discrepancy of the electron affinity of oxygen with the value admitted so far, 11 784.648(6) cm^{-1}, is yet unexplained. [S1050-2947(99)12305-9]

PACS number(s): 32.80.Gc, 32.10.Hq, 03.75.−b, 07.78.+s

I. PHOTODETACHMENT MICROSCOPY AND ELECTRON SPECTROMETRY

Photodetachment microscopy, as explained in recent papers [1,2], deals with photodetachment of atomic anions in the presence of a uniform electric field. It consists of looking at the spatial distribution of the electrons that come out the ions around the electric-field axis. The electron spot has an internal structure, which can be interpreted as an interference pattern in the semiclassical approximation. In a rigorous quantum description, the electron pattern appears as the bound factor of the electron wave function in the detachment continuum.

Interference, if we consider it in this way, takes place between two half electron waves, one which escapes from the ion directly in the downfield direction, and another which is emitted in the upfield direction and then undergoes reflection by the homogeneous field. The resulting ring pattern can be observed, provided that (i) the initial kinetic energy ε at which the electron is brought above the detachment threshold is low enough, namely, in the 0.1–3-cm^{-1} range; (ii) the electric field correspondingly remains in the 10^2-10^4 $V\,m^{-1}$ range; and (iii) one uses a high spatial resolution electron detector [1,2].

In the original proposal to build a photoionization or photodetachment microscope [3], one can already find the idea that measuring the pattern radius at a single value of the energy could be enough to determine the electron energy; hence the ionization or detachment threshold, in contrast with current methods, for instance extrapolation from Rydberg series, that have to exploit data from a whole energy interval. The radius of the spot increases as $\varepsilon^{1/2}$.

One can also measure the accumulated phase $\Delta\Phi$ of the interference pattern, which can be calculated semiclassically as $\hbar^{-1}$ times the reduced action difference ΔS between the two extreme trajectories, both of which start parallel to the electric field, in opposite directions, and end on the center of the electron spot. Equivalently, one can measure the number of rings $N=h^{-1}\Delta S$. Both $\Delta\Phi$ and N have a $\varepsilon^{3/2}$ variation with the energy, which makes them more sensitive to energy variations than the spot radius. They are also dimensionless quantities, which means that phase or N measurements do not require an absolute calibration of the electron image sizes. Measuring N is just a matter of counting bright and dark rings.

A rigorous quantitative analysis is made, much more precisely, by fitting the quantum formula for the radial oscillation of the electron current [4] with the experimental data. Nevertheless the conclusion remains that matching the radial oscillation becomes so strong a criterion that any concern due to the uncertainty on the pixel size can be eliminated. Photodetachment microscopy thus brings a qualitative improvement due to its interferometric character when compared to classical electron spectrometry, even when done by electric-field photoelectron imaging [5,6].

II. QUANTITATIVE PHOTODETACHMENT MICROSCOPY AND DOPPLER EFFECT

The interferometric analysis however relies on the theoretical formula that gives the accumulated phase as a function of the initial kinetic energy ε [7],

$$\Delta\Phi=\frac{4\sqrt{2}}{3}\frac{\sqrt{m}}{\hbar qF}\varepsilon^{3/2}, \tag{1}$$

with q the elementary charge, m the electron mass, and F the applied electric field.

This formula is, strictly speaking, valid only in the free-electron case, i.e., for the case where the electron can be considered as a free one just after it has been detached. Deviations from this situation could well change the phase vs energy function in an appreciable way. The electron energy that can be obtained by fitting Eq. (1) to the experimental O^- interferograms has nevertheless always appeared as a linear function of the laser energy [2]. This has made us confident that scattering of the freed electron by the residual atomic core can be considered negligible, at least as far as photodetachment of light anions like oxygen is concerned, and that ε, as it comes from the fitting procedure, is the actual initial kinetic energy of the electron, with A the electron affinity of the atom and $h\nu$ the photon energy: $\varepsilon=h\nu-A$.

Even if the initial kinetic energy ε of the freed electron can be determined with a high accuracy, this is of little help for determining the electron affinity $A=h\nu-\varepsilon$ when one does not know the energy $h\nu$ of the excitation photon pre-

cisely. Trouble comes from the fact that $h\nu$ has to be measured in the ion's rest frame, which is usually a fast-moving one. With a kinetic energy of 500 eV only, our O^- ions still have a velocity V of about 77 km s^{-1} with respect to the light source. We endeavor to illuminate the ion beam at right angles, in order to bring the Doppler shifting as close to zero as possible, but an uncertainty remains which is related to the intersection angle uncertainty by a 0.053 cm^{-1}/deg factor, much too large to compete with the accuracy of the last measurement of the oxygen electron affinity: 11 784.648(6) cm^{-1} [8,9].

Alternatively, the laser and ion beams can be merged together, in parallel and antiparallel configurations successively, which makes the Doppler shift take its extreme values, and sets the Doppler broadening to zero at first order. The electron affinity of oxygen was measured using these configurations [8]. They are, however, incompatible with photodetachment microscopy, for a small photodetachment volume is needed in order not to blur the electron interference pattern completely. We thus slightly modified the laser-at-right-angles scheme in order to make a double pass possible. A compromise is achieved, by which electron spots can still be analyzed as interference patterns and the Doppler unknown can be eliminated, as explained below.

III. EXPERIMENTAL SETUP FOR DOUBLE-PASS PHOTODETACHMENT MICROSCOPY

The same highly collimated ion beam of O^- is used as previously [2]. Briefly, O^- ions are produced in a hot cathode discharge source, which is fed with a gaseous mixture of Ar (80%) and N_2O (20%). All the negative ions that are produced by the discharge are extracted with a 1200-eV kinetic energy. A Wien velocity filter makes it possible to select either the most abundant isotope $^{16}O^-$, or the heavier isotope $^{18}O^-$. A decelerator brings the O^- ion kinetic energy down to 500 eV just before the ion beam enters the interaction region through a 1.7- or 1.3-mm aperture.

Photodetachment is produced with a sapphire-titanium laser, at a wavelength slightly smaller than the threshold wavelength, $\lambda = 848.33$ nm for O^-. Because the center of the electron spot on the detector is just the projection of the position from where the ion was detached in the laser beam, the spatial definition of the electron image cannot be better than the area of the laser and ion-beam intersection, as it appears when observed in the electric-field direction. This was the reason why the laser was passed quasiparallel to the electric field, when we just aimed at obtaining the best possible spatial resolution for photoelectron images [2]. Focusing the laser in such a configuration actually resulted in a minimum area of the interaction region, as seen in the detection direction.

The exact value of the intersection angle between the laser and ion beam cannot be known very precisely, however. The laser, being focused by a 0.27-m lens, has a focal spot with a waist parameter of about 19 μm on the ion beam, and hence a total divergence of 28 mrad (1.6°), which makes it difficult to measure the mean laser beam direction, even at far distances, with an accuracy better than 1°. Moreover, the ion beam does not exactly follow the horizontal axis of the experimental chamber. Negative ions undergo an electrostatic force, as soon as they enter the electric-field region. Trouble comes from the fact that the electric field cannot be made uniform at the very entrance of the interaction chamber, with a strong dependence on the exact ion beam transverse position. This drawback prevents us from predicting the exact ion-beam incidence, when it reaches the interaction volume, with an accuracy better than 1°.

A high accuracy measurement of the detachment threshold thus requires some additional information, in order to eliminate the unknown Doppler angle. A double-pass scheme of the laser onto the ion beam can classically be used in laser photodetachment threshold measurements [10]. If the two light beams are exactly antiparallel, which is easily achieved by reflecting the beam in a corner cube, the photodetachment signals undergo symmetric Doppler shifting. The two apparent thresholds can then easily be averaged, in order to yield a Doppler-free detachment threshold wave number, at least to the first order of Doppler corrections. Merging the laser with the ion beam, in the same direction and in opposite directions successively, may appear as the most elegant technique, for Doppler broadening is minimized and Doppler correction can be achieved at all orders by direct geometrical averaging of the two positively and negatively shifted wave numbers. However, the identity of the ion-beam velocity during the two measurements must be guaranteed to a high precision, in order not to introduce a systematic shift of the result. The presently admitted experimental value of the electron affinity of oxygen was obtained in the merged-beam configuration [8], but for the geometrical averaging, which led to a later correction [9].

Passing a focused light beam forth and back across the ion beam without refocusing requires reflection to be made within one Rayleigh length Z_R from one crossing to the other, along the light path. Numbers immediately show that it is impossible with as strong a focusing as before, for $w_0 \cong 19\,\mu$m gives a Rayleigh length $Z_R \cong 1.4$ mm only. Another beam setting was tried, with a larger focal length focussing lens, which increased the Rayleigh length to $Z_R \cong 0.47$ m. This is about the minimum Rayleigh length that makes it possible to keep a relatively well-focused beam after it has been reflected outside the vacuum chamber. The corresponding focal waist is however already so large, $w_0 \cong 357\,\mu$m, and the spatial resolution consequently so poor, that no electron interference pattern could be observed any longer.

Parallel reflection of the laser onto the ion beam was thus abandoned, the laser beam was refocused onto the ion beam by an $f = 200$ mm concave mirror, according to the sketch perspective of Fig. 1. Every intersection of the laser with the ion beam produces an independent electron spot on the detector. Since the transverse shift the spots undergo due to the initial ion velocity does not depend on their starting point, the distance between the electron spots is a direct measurement of the distance D of the two interaction zones.

The electron pictures produced by the incident (i) and reflected (r) beams will be analyzed, as explained below, to give the initial kinetic energy E_i or E_r (respectively) of the emitted electron in the ions' rest frame. The recoil energy of the electron plus atom ensemble due to the momentum of the absorbed photon is negligible, less than 10^{-6} cm^{-1}. The recoil energy of the atom with respect to the freed electron, in

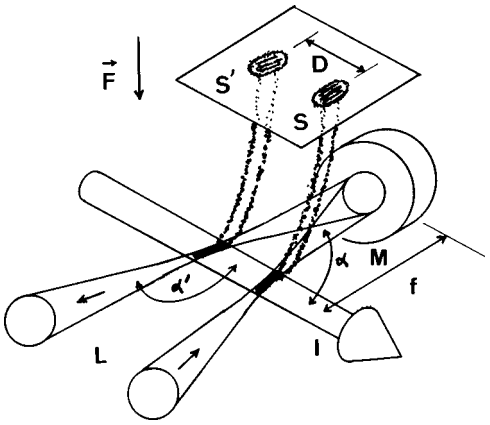

FIG. 1. Perspective drawing of the double-pass experimental setup, showing how electron spots S and S' become elongated, due to the shape of the intersection volumes (in black) of the laser L with the ion beam I, the diameter of which is about 0.6 mm. Doppler angles α and α' are the angles between the mean velocity vector of the ions and the propagation directions of the laser, before and after reflection, respectively. Since the Doppler shift only depends on their cosine, they are always taken as positive angles. Distance D between the interaction zones and between the spots is positive (negative) in the case of a positive (negative) Doppler shift, i.e., an intersection of the ion beam with the reflected laser upstream (downstream) of the intersection with the incident laser. Angle D/f, f being the focal length of the mirror M, is exaggerated.

the center-of-mass frame, can also be neglected, for it is less than 4×10^{-5} times the electron kinetic energy. For practical purposes, we may thus consider that all of the excess energy $h\nu-A$ is transferred to the electron kinetic energy.

Now the photon energy has to be estimated in the ions' rest frame. With intersection angles α and α' defined as on Fig. 1, E_i and E_r kinetic energies can be expressed as functions of the laboratory laser frequency ν with the usual relativistic parameters $\beta=V/c$ and $\gamma=(1-\beta^2)^{-1/2}$ by $E_i=\gamma(1-\beta\cos\alpha)h\nu-A$ and $E_r=\gamma(1-\beta\cos\alpha')h\nu-A$, respectively.

Averaging then yields

$$A=\gamma\left(1-\beta\cos\frac{\alpha+\alpha'}{2}\cos\frac{\alpha-\alpha'}{2}\right)h\nu-\frac{E_i+E_r}{2}. \quad (2)$$

If α and α' are defined as positive angles, $(\alpha-\alpha')/2$ is very nearly zero, which gives a cosine practically equal to 1. On the other hand, the three angles of the triangle made by the two laser–ion-beam intersections and the reflection point on the mirror must satisfy the sum rule, hence $(\alpha+\alpha')/2=\pi/2+D/2f$. Formula (2) can thus be simplified into

$$A=\gamma\left(1+\beta\frac{D}{2f}\right)h\nu-\frac{E_i+E_r}{2}. \quad (3)$$

Here again, the ratio D/f being always of the order of 10^{-2}, we can estimate that the error due to the approximations made on the sine and cosine values will never exceed 2×10^{-8} times the photon energy, or $3\times10^{-4}\,\mathrm{cm}^{-1}$, and can be neglected. Formula (3) thus provides us with a way to determine the electron affinity A without any absolute measurement of the intersection angle, the only required measurement being the distance between the forth and back interaction zones. Uncertainty on this value will of course be included in the final result.

A symmetric configuration can also be used, in which the reflected laser beam crosses the ion beam downstream of the incident laser beam. The Doppler shift is then, on average, a negative one, and formula (3) will simply be replaced by

$$A=\gamma\left(1-\beta\frac{D}{2f}\right)h\nu-\frac{E_i+E_r}{2}. \quad (4)$$

No confusion can occur practically between the two configurations, for the difference $\gamma\beta(D/f)h\nu$ is too large, of the order of 0.03 cm^{-1}, to remain undetected.

IV. PHOTOELECTRON IMAGES AND DATA ANALYSIS

Figure 2 shows an example of an electron image recorded in the double-crossing configuration. Every spot is the convolution of the ideal ring pattern [2] with the transverse section of the interaction volume. Since here the laser propagates at right angles with the electric field, the convolution is very anisotropic. Spatial resolution is completely lost in the light propagation direction, but a modulation of the electron current remains in the transverse direction, which is enough to count the rings of the underlying ring pattern or, more rigorously, to fit the data for a precise determination of the interferogram phase. In order to make the fitting calculation tractable, the data are first reduced to a one-dimensional profile by integrating the photocurrent over every pixel column. A lot of time is thus gained, with nearly no loss of information, essentially by getting rid of numerous recalculations of a slowly converging two-dimensional convolution, and reducing the number of points to be fitted from several thousand to less than one hundred.

Because of the existence of a fine structure, both of the neutral atom O and of the negative ion O^-, as represented in Fig. 3, six different fine-structure detachment thresholds can be studied, that we label from A to F in the order of increasing detachment energies. The true detachment threshold, at 848.33 nm, from ground state O^- to ground state neutral O is threshold C. The fine-structure splitting of neutral oxygen is so well known, with energy intervals of $^3P_2$ to $^3P_1$ and $^3P_1$ to $^3P_0$ equal to 158.268 74 and 68.716 49 cm^{-1} in ^{16}O, respectively [11], that subtracting them from threshold E and F energies yields an electron affinity measurement as reliable as the direct measurement of threshold C. Figure 4 shows a histogram of the experimental results, with an identification of the method used for each of them. No significant deviation appears that would indicate that one method yields a different result from another.

V. EXPERIMENTAL UNCERTAINTIES

A. Wave-number measurement

Our electron affinity measurements rely on an accurate measurement of the wave number of the excitation laser. This is done by a lambdameter, i.e., a symmetrical Michelson interferometer, in which the sapphire-titanium wavelength is compared to the reference wavelength of a I_2-saturated absorption stabilized He-Ne laser. Several hyper-

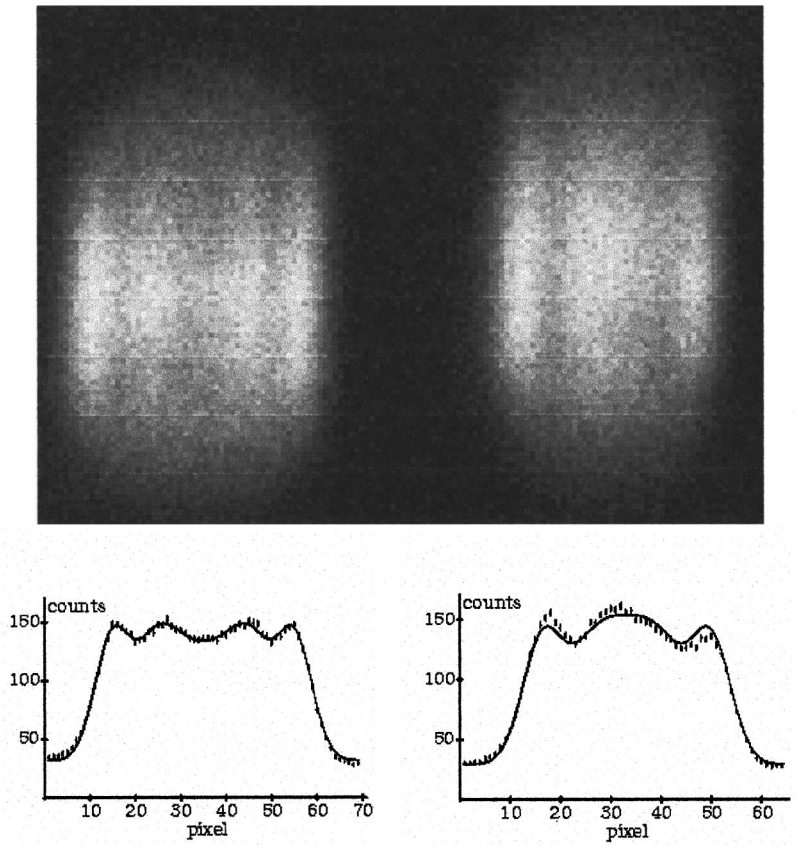

FIG. 2. Example of a pair of electron images in the positive average Doppler shifting case. The histogram of the average numbers of electron counts per pixel is given under every image. The continuous line is the result of the fitting process applied to these histograms.

fine components of the $^{127}I_2$ $R(127)$ line can be used, all of which have been measured with an extremely good accuracy. We usually lock the reference laser on the g component, the wave number of which is 15 798.007 18 cm^{-1} [12].

The lambdameter computes the unknown laser wavelength by multiplying the reference wavelength by the measured ratio of both wavelengths. But the interferometer is operated in room atmosphere. If the air index were the same for both wavelengths, the desired wavelength in vacuum would be obtained simply by using the He-Ne wavelength in vacuum as the lambdameter input. This would overestimate the IR wavelength vacuum by the ratio of the air indices $n(632.8\,\text{nm})/n(848.3\,\text{nm}) \cong 1.000\,001\,76$ [13]. The proper

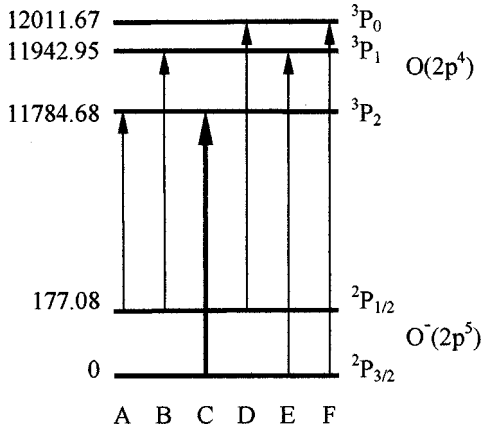

FIG. 3. Fine structure of O^- and neutral O, with the definition of the six ''fine-structure detachment thresholds'' labeled A, B, C, D, E, and F, in the order of increasing transition energies. Fine-structure intervals are magnified with respect to the transition energy, both for the negative ion and the neutral atom, by a common factor. Energies are measured in cm^{-1}.

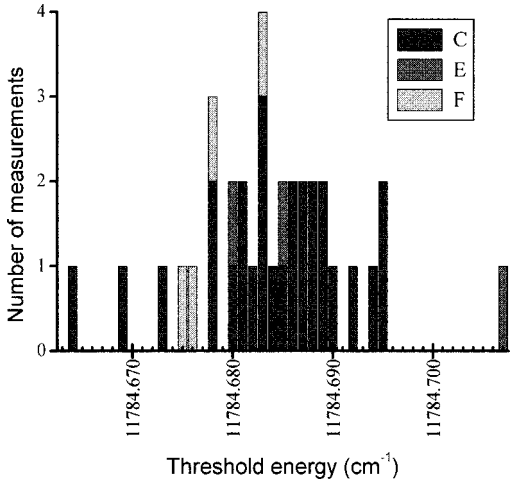

FIG. 4. Histogram of obtained energies for the detachment threshold of O^-. Most measurements were done by double-pass photodetachment microscopy at threshold C. A few measurements were also done just above thresholds E and F, the obtained energies of which can be corrected by the fine-structure intervals of O to yield another value of threshold C energy. The obtained average value, before systematic corrections are applied, is 11 784.683 cm^{-1} with a standard deviation of 0.008 cm^{-1}.

reference wavelength for the lambdameter is thus the vacuum wavelength of the g component of the $R(127)$ iodine line divided by the former ratio, namely 632 990.116 pm. The measured wave numbers, such as the set represented in Fig. 4, have been determined using this reference.

The room atmosphere is not, however, standard air. We did not record day-to-day atmospheric pressure fluctuations, but on average, the Laboratoire Aimé-Cotton being at a 150-m elevation above sea level, the (air index -1) difference should be lowered by about 2%. A systematically higher temperature, in the interferometer with respect to the standard 15 °C condition, results in additional lowering of the air density by about 4%. The standard air index ratio is thus an overestimated value, and we can expect the true IR wavelengths in vacuum to be larger by 10^{-7} than what the lambdameter directly tells. The corresponding correction to be applied to wave numbers will be $-1.2\times10^{-3}\,\mathrm{cm}^{-1}$. A similar result is obtained by directly computing the respective air indices using Edlén's formula [14].

The exactness of the wave-number measurement was tested in a saturated-absorption spectroscopy experiment in Cs vapor. The sapphire-titanium laser was successively tuned to eight different—two-level and crossover—hyperfine components of the D_2 resonance line of ^{133}Cs, the wavelength of which, about 852 nm, is close to the detachment wavelength of O^-. Eleven independent measurements of the laser wavelength were performed with the lambdameter. Taking into account the air density correction just described and the air index ratio at the two different wavelengths 848 and 852 nm, we obtain results that differ from the known wavelengths of the D_2 line [15] by -0.01 pm on average, with a standard deviation of 0.02 pm. Conditions for this test were actually favorable, for on the day of the measurement the atmospheric pressure in the Orsay area, reduced to sea level, was actually close to the standard 1013 hPa [16].

Even if the Cs resonance line test shows a wave number deviation smaller than $2\times10^{-4}\,\mathrm{cm}^{-1}$, this excellent agreement may partly be due to chance. The test measurements, like all wavelength measurements, are obtained by averaging over a series of wavelength outputs, the standard deviation of which sometimes appears to be as large as 0.1 pm, i.e., in wave-number units, $1.4\times10^{-3}\,\mathrm{cm}^{-1}$. We cannot rule out the possibility that, on certain days, a systematic shift of the average measurement occurs which is of the same order of magnitude. A careful estimate of the possible final error due to wavelength measurements should thus be a $\pm2\times10^{-3}$ cm^{-1} interval.

B. Electric-field determination

According to formula (1), what photodetachment microscopy measures is only a $\varepsilon^{3/2}/F$ ratio. Uncertainty on the electric-field determination will thus produce some systematic uncertainty on the kinetic-energy measurement. The applied voltage that makes the uniform electric field is determined with a $\pm0.2\%$ accuracy. The uniformity of the resistors that divide this applied voltage, especially in the interaction region, is guaranteed at a $\pm0.1\%$ level. The spacing between adjacent parallel electrostatic plates, especially the spacing of the pair around the interaction region, should obey a $\pm0.6\%$ accuracy. The electric-field value is thus known with a $\pm0.9\%$ accuracy. This results in a systematic uncertainty about the electron initial kinetic energy of $\pm0.6\%$, for measurements that essentially dealt with energies in the 0.6–0.8 cm^{-1} range. The possible systematic error due to an electric-field deviation from the assumed value is thus within a $\pm5\times10^{-3}$ cm^{-1} interval.

C. Image scaling uncertainty

As explained in Sec. I, counting fringes, rather than making spot size measurements, determines the nominal energy ε of the interferogram. But the absolute pixel size plays a role in formulas (3) and (4), when the distance between the two electron spots is used to eliminate the first-order Doppler effect. The pixel size is known with a $\pm2\%$ accuracy, which results in an additional $\pm4\times10^{-4}$ cm^{-1} uncertainty on the electron affinity. The effect is partially compensated for by the fact that the two types of double-pass experiments, either with a positive or a negative average Doppler shift, are affected oppositely by a given change of the pixel size. The fact that no systematic shift appears, at a 10^{-3} cm^{-1} scale, between electron affinities obtained either in the positive, or negative setting of the beam makes us rather confident on the assumed pixel size of 26 μm.

D. Kinetic-energy uncertainty

Finally, the absolute ion velocity also plays a role in formulas (3) and (4). A $\pm1\%$ uncertainty on the ion kinetic energy results in a $\pm0.5\%$ uncertainty in the first-order Doppler correction. This means another $\pm10^{-4}$ cm^{-1} uncertainty on the final result. That would be $\pm15\times10^{-3}\,\mathrm{cm}^{-1}$ in collinear spectroscopy.

VI. RESULTS

A. ^{16}O and ^{18}O electron affinities

The final result, after the -1.2×10^{-3} cm^{-1} atmospheric pressure correction has been taken into account, is $A(^{16}\mathrm{O}) = 11\,784.682(20)\,\mathrm{cm}^{-1}$, in which $\pm12\times10^{-3}\,\mathrm{cm}^{-1}$ has been set as a conservative estimate of the maximum statistical dispersion of a series of measurements. For the heavier isotope, experiments take a much longer time, so statistics are significantly poorer. We obtain $A(^{18}\mathrm{O}) = 11\,784.612(29)\,\mathrm{cm}^{-1}$. The isotope shift of the electron affinity of oxygen, ^{18}O with respect to ^{16}O, is then $-0.070(27)\times10^{-3}\,\mathrm{cm}^{-1}$. Uncertainty appears to be reduced here because the unknown error made when measuring the electric field is the same in both measurements, and can be eliminated from the error on the affinity difference.

A negative isotope shift is an anomalous one. If one considers that every electron independently induces nuclear recoil, one expects a ''normal mass shift'' which is always positive, from the lighter to the heavier isotope, whatever the atomic transition [17]. In oxygen, the normal mass shift from the ^{16}O to the ^{18}O electron affinity, would be 0.045 cm^{-1}. The normal-mass shift has to be corrected by the fact that electron correlations can either amplify or reduce the nuclear recoil with respect to the independent-electron picture. This is the ''specific mass shift,'' the calculation of which is much more difficult, because it depends on the details of the appropriate wave functions. Because nuclear volume effects are

very small in light atoms or ions, the isotope shift can be considered as being just the sum of the normal and specific mass shifts. In this approximation, we have a specific mass shift of $-0.115(27)$ cm^{-1}.

We lack theoretical results that would make a quantitative comparison possible, though the electron affinity of oxygen was the subject of many calculations in recent years [18]. Hyperfine structures in neutral oxygen were the subject of high-resolution spectroscopy experiments [19] and of multiconfiguration Hartree-Fock (MCHF) calculations [20]. As for isotope shifts, some results obtained by MCHF calculations were recently reported in boron and carbon [21]. These, together with the present electron affinity result, could motivate a specific theoretical investigation of isotope shifts in O^-.

As concerns experimental data, very few isotope shifts are known in negative ions, though studying the specific mass shifts can be a way to learn more about the electron correlations, which are known to play an important role in negative ion stability. In the H^--D^- pair, the electron affinity isotope shift is 3.2 (7) cm^{-1} [22]. The $^1P^0$ resonances that lie below the H($n=2$) threshold also exhibit a positive isotope shift [23]. The detachment threshold isotope shift from $^{35}Cl^-$ to $^{37}Cl^-$ is positive, 0.007 (5) cm^{-1}, but its smallness reveals a negative, -0.017 (5) cm^{-1}, specific mass shift [24]. In Br^-, the 79–81 detachment threshold isotope shift was found smaller than the 10^{-2}-cm^{-1} resolution of the experiment [10].

B. Fine structure of $^{16}O^-$

In a way similar to what is performed for the ''true'' $^2P_{3/2}$–$^3P_2$ threshold C, photodetachment microscopy measurements at thresholds A, B, and D (Fig. 3) can be put together to provide us with an experimental value of the $^2P_{1/2}$–$^3P_2$ transition energy. The result is $A(^{16}O\ ^3P_2 - ^{16}O^-\ ^2P_{1/2}) = 11\,607.597(29)$ cm^{-1}. Subtraction of this energy from the true electron affinity yields the $^2P_{1/2}$-$^2P_{3/2}$ fine structure of the $^{16}O^-$ negative ion, 177.085 (27) cm^{-1}, which is close to the previously admitted value, 177.08 (5) cm^{-1} [25], with an error bar reduced by a factor of 2.

VII. CONCLUSION

Photodetachment microscopy has been applied to the case of O^-, in a double-pass configuration that allows us to eliminate the largest part of the first-order Doppler shift. The electron affinities of ^{16}O and ^{18}O have been measured, together with the fine structure of the negative ion $^{16}O^-$. Whereas the fine-structure result perfectly agrees with the previously published value, the electron $A(^{16}O) = 11\,784.682(20)$ cm^{-1} significantly differs from the admitted value $A(^{16}O) = 11\,784.648(6)$ cm^{-1} [8,9], even though we endeavored not to overestimate the accuracy of our electron affinity measurement.

This discrepancy can be seen as a serious question about the experimental technique. We of course checked the proper operation of the magnetic shielding, and found a magnetic field inside the interaction chamber lower than 3 μT. The corresponding cyclotron energy is 3×10^{-6} cm^{-1}. The increase of the detachment energy that would be due to a Landau structure of the detachment continuum is thus four orders of magnitude too small to offer an explanation. The finite radius of the initial ion may also induce a shift of the detachment threshold with respect to the ideal pointlike source picture, but assuming a 0.14-nm radius and a 423-V m^{-1} field, the shift is -5×10^{-4} cm^{-1} only. No explanation, in terms of a systematic energy shift, is found about the present experiment that could explain the electron affinity discrepancy found.

The electron energy measurement here relies on a technique that makes use of the sensitivity of the electron interference pattern to the experimental parameters. The initial kinetic energy is only one of these. The possibility cannot be excluded that the interference state of the outgoing electron wave depend in a non-negligible way on transverse magnetic or electric fields, even when those fields are not strong enough to produce direct energy shifts. More sophisticated calculations for nonperfect cases of photodetachment microscopy, and more experiments, are thus required to check the robustness of the photoelectron interferogram against spurious magnetic or electric-field components or electric-field inhomogeneities. New photodetachment experiments could also lead to interesting comparisons, if performed on other negative ions, the detachment energies of which have been determined independently.

ACKNOWLEDGMENTS

The authors gratefully acknowledge the lending of a saturated-absorption stabilized He-Ne laser by Patrick Juncar, at the Conservatoire National des Arts et Métiers, Paris, and operation of this laser by Bruno Viaris. The saturated absorption test on Cs vapor was efficiently performed thanks to Andrea Fioretti's expertise on atomic Cs spectroscopy. Laboratoire Aimé-Cotton is a laboratory of the Centre National de la Recherche Scientifique, UPR 3321, associé à l'Université Paris–Sud.

[1] C. Blondel, C. Delsart, and F. Dulieu, Phys. Rev. Lett. **77**, 3755 (1996).

[2] C. Blondel, C. Delsart, F. Dulieu, and C. Valli, Eur. Phys. J. D **2**, 207 (1999).

[3] Yu. N. Demkov, V. D. Kondratovich, and V. N. Ostrovskii, Pis'ma Zh. Eksp. Teor. Fiz. **34**, 425 (1981) [JETP Lett. **34**, 403 (1981)].

[4] V. D. Kondratovich and V. N. Ostrovsky, J. Phys. B **23**, 3785 (1990).

[5] H. Helm, N. Bjerre, M. J. Dyer, D. L. Huestis, and M. Saeed, Phys. Rev. Lett. **70**, 3221 (1993).

[6] D. H. Parker and A. T. J. B. Eppink, J. Chem. Phys. **107**, 2357 (1997).

[7] C. Bracher, W. Becker, S. A. Gurvitz, M. Kleber, and M. S.

Marinov, Am. J. Phys. **66**, 38 (1998).
[8] D. M. Neumark, K. R. Lykke, T. Andersen, and W. C. Lineberger, Phys. Rev. A **32**, 1890 (1985).
[9] C. Blondel, Phys. Scr. **58**, 31 (1995).
[10] C. Blondel, P. Cacciani, C. Delsart, and R. Trainham, Phys. Rev. A **40**, 3698 (1989).
[11] P. De Natale, M. Bellini, W. Goetz, M. Prevedelli, and M. Inguscio, Phys. Rev. A **48**, 3757 (1993).
[12] T. J. Quinn, Metrologia **30**, 523 (1994).
[13] C. DeWitt Coleman, W. R. Bozman, and W. F. Meggers, *Table of Wavenumbers*, Natl. Bur. Stand. (U.S.) Monograph No. 3 (U.S. GPO, Washington, DC, 1960), Vols. I and II.
[14] K. P. Birch and M. J. Downs, Metrologia **31**, 315 (1994).
[15] G. Carlsson, A. Kastberg, and L. R. Pendrill, Metrologia **34**, 387 (1986).
[16] Atmospheric pressure in the afternoon of 17 October 1997 was about 1015 hPa, as recorded on the Brétigny aerodrome, courtesy of Météo-France, Centre d'Essais en Vol, F-91228 Brétigny-sur-Orge.
[17] W. H. King, *Isotope Shifts in Atomic Spectra* (Plenum, New York, 1984).
[18] D. Feller and E. R. Davidson, J. Chem. Phys. **90**, 1024 (1989); T. Noro, M. Yoshimine, M. Sekiya and F. Sasaki, Phys. Rev. Lett. **66**, 1157 (1991); R. A. Kendall and T. H. Dunning, Jr., J. Chem. Phys. **96**, 6796 (1992); D. L. Strout and G. E. Scuseria, *ibid.* **96**, 9025 (1992); B. S. Jursic, *ibid.* **104**, 4151 (1996); G. Miecznik and C. H. Greene, Phys. Rev. A **53**, 3247 (1996).
[19] M. de Angelis, M. Inguscio, L. Julien, F. Marin, A. Sasso, and G. M. Tino, Phys. Rev. A **44**, 5811 (1991); F. Marin, C. Fort, M. Prevedelli, M. Inguscio, G. M. Tino, and J. Bauche, Z. Phys. D **25**, 191 (1993).
[20] M. R. Godefroid, G. Van Meulebeke, P. Jönsson, and C. Froese Fisher, Z. Phys. D **42**, 193 (1997).
[21] P. Jönsson, C. Froese Fisher, and M. R. Godefroid, J. Phys. B **29**, 2393 (1996).
[22] K. R. Lykke, K. K. Murray, and W. C. Lineberger, Phys. Rev. A **43**, 6104 (1991).
[23] H. H. Andersen, P. Balling, P. Kristensen, U. V. Pedersen, S. A. Aseyev, V. V. Petrunin, and T. Andersen, Phys. Rev. Lett. **79**, 4770 (1997).
[24] U. Berzinsh, M. Gustafsson, D. Hanstorp, A. Klinkmüller, U. Ljungblad, and A. M. Martensson-Pendrill, Phys. Rev. A **51**, 231 (1995).
[25] H. Hotop and W. C. Lineberger, J. Phys. Chem. Ref. Data **14**, 731 (1985).